

Deep Discriminative to Kernel Density Networks for Calibrated Inference

Jayanta Dey,^{1,*} Will LeVine,^{1,2} Haoyin Xu,^{1,†} Ashwin De Silva,^{1,†} Tyler M. Tomita,¹ Ali Geisa,¹
Tiffany Chu,¹ Jacob Desman,¹ and Joshua T. Vogelstein¹

Abstract. Deep discriminative approaches like random forests and deep neural networks have recently found applications in many important real-world scenarios. However, deploying these learning algorithms in safety-critical applications raises concerns, particularly when it comes to ensuring confidence calibration for both in-distribution and out-of-distribution data points. Many popular methods for in-distribution (ID) calibration, such as isotonic regression and Platt’s sigmoidal regression, exhibit excellent ID calibration performance but often at the cost of classification accuracy. Moreover, these methods are not calibrated for the entire feature space, leading to overconfidence in the case of out-of-distribution (OOD) samples. In this paper, we leveraged the fact that deep models, including both random forests and deep-nets, learn internal representations which are unions of polytopes with affine activation functions to conceptualize them both as partitioning rules of the feature space. We replace the affine function in each polytope populated by the training data with a Gaussian kernel. We propose sufficient conditions for our proposed methods to be consistent estimators of the corresponding class conditional densities. Moreover, our experiments on both tabular and vision benchmarks show that the proposed approaches obtain well-calibrated posteriors while mostly preserving or improving the classification accuracy of the original algorithm for in-distribution region, and extrapolates beyond the training data to handle out-of-distribution inputs appropriately.

1 Introduction Machine learning methods, specially deep neural networks and random forests have shown excellent performance in many real-world tasks, including drug discovery, autonomous driving and clinical surgery. However, calibrating confidence over the whole feature space for these approaches remains a key challenge in the field. Although these learning algorithms can achieve near optimal performance at inferring on the samples lying in the high density regions of the training data [1–3], they yield highly confident predictions for the samples lying far away from the training data [4]. Calibrated confidence within the training or in-distribution (ID) region as well as in the out-of-distribution (OOD) region is crucial for safety critical applications like autonomous driving and computer-assisted surgery, where any aberrant reading should be detected and taken care of immediately [4, 5]. A well-calibrated model capable of quantifying the uncertainty associated with inference for any points from the training distribution as well as detecting OOD data can be a life-saver in these cases.

The approaches to calibrate OOD confidence for learning algorithms described in the literature can be roughly divided into two groups: discriminative and generative. Discriminative approaches try to scale the posteriors based on OOD detection or modify the learning loss function. Intuitively, the easiest solution for OOD confidence calibration is to learn a function that gives higher scores for in-distribution samples and lower scores for OOD samples, and thereby re-scale the posterior or confidence score from the original model accordingly [6]. There are a number of approaches in the literature which try to either modify the loss function [7–9] or adversarially train the network to be less confident on OOD samples [4, 10]. Recently, as shown by Hein et al. [4], the `ReLU` networks produce arbitrarily high confidence as the inference point moves far away from the training data. Therefore, calibrating `ReLU` networks for the whole OOD region is not possible without fundamentally changing the network architecture. As a result, all of the aforementioned algorithms are unable to provide any guarantee about the performance of the network through out the whole feature space. On the other end of the spectrum, the generative group tries to learn generative models for both the in-distribution as well as the out-of-distribution samples. The general idea is to conduct likelihood ratio tests for a particular sample out of the generative models [11], or threshold the ID likelihoods to determine OOD samples. However, it is not obvious how to control likelihoods far away from the training data for powerful generative models

¹ Johns Hopkins University (JHU), ²Scale AI

* corresponding author: jdey4@jhu.edu

like variational autoencoders (VAEs) [12] and generative adversarial networks (GAN) [13]. Moreover, Nalisnick et al. [14] and Hendrycks et al. [10] showed VAEs and GANs can also yield overconfident likelihoods far away from the training data.

The algorithms described so far are concerned with OOD confidence calibration for deep-nets only. However, in this paper, we show that other approaches which partition the feature space, for example random forest, can also suffer from poor confidence calibration both in the ID and the OOD regions. Moreover, the algorithms described above are concerned about the confidence of the algorithms in the OOD region only and they do not address the confidence calibration within the training distribution at all. This issue is addressed separately in a different group of literature [15–20]. In this paper, we consider both calibration problem jointly and propose an approach that achieves good calibration throughout the whole feature space.

In this paper, we conceptualize both random forest and ReLU networks as partitioning rules with an affine activation over each polytope. We consider replacing the affine functions learned over the polytopes with Gaussian kernels. We propose two novel kernel density estimation techniques named *Kernel Density Forest* (KDF) and *Kernel Density Network* (KDN). We theoretically show that they asymptotically converge to the true training distribution under certain conditions. At the same time, the estimated likelihood from the kernel density models decreases for samples far away from the training samples. By adding a suitable bias to the kernel density estimate, we can achieve calibrated posterior over the classes in the OOD region. It completely excludes the need for providing OOD training examples to the model. We conduct several simulation and real data studies that show both KDF and KDN are robust against OOD samples while they maintain good performance in the in-distribution region.

2 Related Works and Our Contributions There are a number of approaches in the literature which attempt to learn a generative model and control the likelihoods far away from the training data. For example, Ren et al. [11] employed likelihood ratio test for detecting OOD samples. Wan et al. [8] modified the training loss so that the downstream projected features follow a Gaussian distribution. However, there is no guarantee of performance for OOD detection for the above methods. To the best of our knowledge, only Meinke et al. [5] has proposed an approach to guarantee asymptotic performance for OOD detection. They model the training and the OOD distribution using Gaussian mixture models which enable them to control the class conditional posteriors far away. Compared to the aforementioned methods, our approach differs in several ways:

- We address the confidence calibration problems for both ReLU -nets and random forests from a common ground.
- We address in-distribution (ID) and out-of-distribution (OOD) calibration problem as a continuum rather than two separate problems.
- We provide guarantees for asymptotic convergence of our proposed approach under certain conditions for both ID and OOD regions.
- We propose an unsupervised OOD calibration approach, i.e., we do not need to train exhaustively on different OOD samples.

3 Methods

3.1 Setting Consider a supervised learning problem with independent and identically distributed training samples $\{(\mathbf{x}_i, y_i)\}_{i=1}^n$ such that $(X, Y) \sim P_{X,Y}$, where $X \sim P_X$ is a $\mathcal{X} \subseteq \mathbb{R}^d$ valued input and $Y \sim P_Y$ is a $\mathcal{Y} = \{1, \dots, K\}$ valued class label. We define in-distribution region as the high density region of $P_{X,Y}$ and denote it by \mathcal{S} . Here the goal is to learn a confidence score, $\mathbf{g} : \mathbb{R}^d \rightarrow [0, 1]^K$, $\mathbf{g}(\mathbf{x}) = [g_1(\mathbf{x}), g_2(\mathbf{x}), \dots, g_K(\mathbf{x})]$ such that,

$$(1) \quad g_y(\mathbf{x}) = \begin{cases} P_{Y|X}(y|\mathbf{x}), & \text{if } \mathbf{x} \in \mathcal{S} \\ P_Y(y), & \text{if } \mathbf{x} \notin \mathcal{S} \end{cases}, \quad \forall y \in \mathcal{Y}$$

where $P_{Y|X}(y|\mathbf{x})$ is the posterior probability for class y given by the Bayes formula:

$$(2) \quad P_{Y|X}(y|\mathbf{x}) = \frac{P_{X|Y}(\mathbf{x}|y)P_Y(y)}{\sum_{k=1}^K P_{X|Y}(\mathbf{x}|k)P_Y(k)}, \quad \forall y \in \mathcal{Y}.$$

Here $P_{X|Y}(\mathbf{x}|y)$ is the class conditional density for the training data which we will refer as $f_y(\mathbf{x})$ hereafter for brevity.

3.2 Background and Main Idea Deep discriminative networks partition the feature space \mathbb{R}^d into a union of p affine polytopes Q_r such that $\bigcup_{r=1}^p Q_r = \mathbb{R}^d$, and learn an affine function over each polytope [4, 21]. Mathematically, the class-conditional density for the label y estimated by these deep discriminative models at a particular point \mathbf{x} can be expressed as:

$$(3) \quad \hat{f}_y(\mathbf{x}) = \sum_{r=1}^p (\mathbf{a}_r^\top \mathbf{x} + b_r) \mathbb{1}(\mathbf{x} \in Q_r).$$

For example, in the case of a decision tree, $\mathbf{a}_r = \mathbf{0}$, i.e., decision tree assumes uniform distribution for the class-conditional densities over the leaf nodes. Among these polytopes, the ones that lie on the boundary of the training data extend to the whole feature space and hence encompass all the OOD samples. Since the posterior probability for a class is determined by the affine activation over each of these polytopes, the algorithms tend to be overconfident when making predictions on the OOD inputs. Moreover, there exist some polytopes that are not populated with training data. These unpopulated polytopes serve to interpolate between the training sample points. If we replace the affine activation function of the populated polytopes with Gaussian kernel \mathcal{G} learned using maximum likelihood approach on the training points within the corresponding polytope and prune the unpopulated ones, the tail of the kernel will help interpolate between the training sample points while assigning lower likelihood to the low density or unpopulated polytope regions of the feature space. This may result in better confidence calibration for the proposed modified approach.

3.3 Proposed Model Consider the collection of polytope indices \mathcal{P} which contains the indices of total \tilde{p} polytopes populated by the training data. We replace the affine functions over the populated polytopes with Gaussian kernels $\mathcal{G}(\cdot; \hat{\mu}_r, \hat{\Sigma}_r)$. For a particular inference point \mathbf{x} , we consider the Gaussian kernel with the minimum distance from the center of the kernel to the corresponding point:

$$(4) \quad r_{\mathbf{x}}^* = \underset{r}{\operatorname{argmin}} \|\mu_r - \mathbf{x}\|,$$

where $\|\cdot\|$ denotes a distance. As we will show later, the type of distance metric considered in Equation 4 highly impacts the performance of the proposed model. In short, we modify Equation 3 from the parent ReLU-net or random forest to estimate the class-conditional density as:

$$(5) \quad \tilde{f}_y(\mathbf{x}) = \frac{1}{n_y} \sum_{r \in \mathcal{P}} n_{ry} \mathcal{G}(\mathbf{x}; \mu_r, \Sigma_r) \mathbb{1}(r = r_{\mathbf{x}}^*),$$

where n_y is the total number of samples with label y and n_{ry} is the number of samples from class y that end up in polytope Q_r . We add a bias to the class conditional density \tilde{f}_y :

$$(6) \quad \hat{f}_y(\mathbf{x}) = \tilde{f}_y(\mathbf{x}) + \frac{b}{\log(n)}.$$

Note that in Equation 6, $\frac{b}{\log(n)} \rightarrow 0$ as the total training points, $n \rightarrow \infty$. The confidence score $\hat{g}_y(\mathbf{x})$ for class y given a test point \mathbf{x} is estimated using the Bayes rule as:

$$(7) \quad \hat{g}_y(\mathbf{x}) = \frac{\hat{f}_y(\mathbf{x})\hat{P}_Y(y)}{\sum_{k=1}^K \hat{f}_k(\mathbf{x})\hat{P}_Y(k)},$$

where $\hat{P}_Y(y)$ is the empirical prior probability of class y estimated from the training data. We estimate the class for a particular inference point \mathbf{x} as:

$$(8) \quad \hat{y} = \operatorname{argmax}_{y \in \mathcal{Y}} \hat{g}_y(\mathbf{x}).$$

3.4 Desiderata We desire our proposed model to estimate confidence score \hat{g}_y to satisfy the following two desiderata:

1. **Asymptotic Performance:** We want point-wise convergence for our estimated confidence as $n \rightarrow \infty$, i.e.,

$$\max_{y \in \mathcal{Y}} \sup_{\mathbf{x} \in \mathbb{R}^d} |g_y(\mathbf{x}) - \hat{g}_y(\mathbf{x})| \rightarrow 0.$$

2. **Finite Sample Performance:** We want better posterior calibration for $\hat{g}_y(\mathbf{x})$ both in ID and OOD regions compared to that of its parent model.

We theoretically derive the conditions under which we achieve Desiderata 1 in Section 4. However, we run extensive experiments on various simulation and benchmark datasets in Section 6 to empirically verify that our proposed approach achieves Desiderata 2.

4 Theoretical Results

Theorem 1 (Asymptotic Convergence to the True Distribution). *Consider a partition rule that partitions \mathbb{R}^d into an infinite number of hypercubes of the same size $h_n > 0$. Formally, let $\mathcal{P}_n = \{Q_1, Q_2, \dots\}$ be a partition of \mathbb{R}^d , that is, it partitions \mathbb{R}^d into sets of the type $\Pi_{i=1}^d [\psi_i h_n, (\psi_i + 1)h_n)$, where ψ_i 's are integers. Let n be the total number of samples and n_r be the number of data points within the polytope Q_r . Consider the true probability density f which is estimated using the samples populating the polytopes using Equation 5, denoted as \hat{f} . The conditions for choosing the Gaussian kernel parameters are:*

1. *The center of the kernel can be any point z_r within the polytope Q_r as $n \rightarrow \infty$,*
2. *The kernel bandwidth along any dimension σ_r is any positive number always bounded by the polytope bandwidth h_n as $n \rightarrow \infty$, i.e., $\sigma_r = C_r h_n$, where $0 < C_r < 1$.*

Consider the following assumptions as well:

1. *The polytope bandwidth $h_n \rightarrow 0$ as $n \rightarrow \infty$.*
2. *n grows faster than the shrinkage of h_n , i.e., $n h_n \rightarrow \infty$ in probability as $h_n \rightarrow 0$.*

Given these assumptions, we have that as $n \rightarrow \infty$:

$$(9) \quad \sup_{\mathbf{x} \in \mathbb{R}^d} |f(\mathbf{x}) - \hat{f}(\mathbf{x})| \rightarrow 0,$$

where $|\cdot|$ denotes absolute value of the scalar it operates on.

Proof. Please see Appendix A for the proof. ■

Theorem 2 (Asymptotic OOD Convergence). *Given n independent and identically distributed training samples $\{(\mathbf{x}_i, y_i)\}_{i=1}^n$, we define the distance of an inference point \mathbf{x} from the training points as: $d_{\mathbf{x}} = \min_{i=1, \dots, n} \|\mathbf{x} - \mathbf{x}_i\|$. Here $\|\cdot\|$ denotes a distance as mentioned in Equation 4. Given non-zero and bounded bandwidth of the Gaussians, then we have almost sure convergence for \hat{g}_y as:*

$$\lim_{d_{\mathbf{x}} \rightarrow \infty} \hat{g}_y(\mathbf{x}) \xrightarrow{as} \hat{P}_Y(y).$$

Proof. Please see Appendix A for the proof. ■

Corollary 3. *Given the conditions in Theorem 1 and 2, we have:*

$$\max_{y \in \mathcal{Y}} \sup_{\mathbf{x} \in \mathbb{R}^d} |g_y(\mathbf{x}) - \hat{g}_y(\mathbf{x})| \rightarrow 0.$$

Proof. Using the law of large numbers, we have $\hat{P}_Y(y) = \frac{n_y}{n} \xrightarrow{a.s.} P_Y(y)$ as $n \rightarrow \infty$. The rest of the proof follows from Theorem 1 and 2. ■

Corollary 4. *There exists a class of random forest algorithms which partitions the feature space satisfying the conditions in Theorem 1.*

Proof. Please see Appendix A for the proof. ■

Corollary 5. *There exists a class of deep-net algorithms which partitions the feature space satisfying the conditions in Theorem 1.*

Proof. Please see Appendix A for the proof. ■

5 Model Parameter Estimation

5.1 Gaussian Kernel Parameter Estimation Theorem 1 implies that the Gaussian kernel parameters for each polytope need to maintain two key properties for ensuring asymptotic optimal performance of our proposed approach. We fit Gaussian kernel parameters to the samples that end up in the r -th polytope using maximum likelihood approach. To satisfy the first condition, we set the kernel center as:

$$(10) \quad \hat{\mu}_r = \frac{1}{n_r} \sum_{i=1}^n \mathbf{x}_i \mathbb{1}(\mathbf{x}_i \in Q_r).$$

To satisfy the second condition, we set the kernel covariance matrix as:

$$(11) \quad \hat{\Sigma}_r = \frac{\sum_{i=1}^n \mathbb{1}(\mathbf{x}_i \in Q_r) (\mathbf{x}_i - \hat{\mu}_r) (\mathbf{x}_i - \hat{\mu}_r)^\top + \lambda I_d}{\sum_{i=1}^n \mathbb{1}(\mathbf{x}_i \in Q_r)},$$

where we regularize the Frobenius norm of precision matrix Σ^{-1} so that Σ does not become singular and λ is the regularization parameter. Note that $\hat{\mu}_r$ in Equation 10 resides always within the corresponding polytope Q_r and the estimated Gaussian bandwidth will be bounded by the polytope bandwidth. We constrain our estimated Gaussian kernels to have diagonal covariance matrix and set the off-diagonal elements of $\hat{\Sigma}_r$ to 0.

5.2 Sample Size Ratio Estimation For a high dimensional dataset with low training sample size, the polytopes are sparsely populated with training samples. For improving the estimate of the ratio $\frac{n_{ry}}{n_y}$ in Equation 5, we incorporate the samples from other polytopes Q_s based on the similarity w_{rs} between Q_r and Q_s as:

$$(12) \quad \begin{aligned} \left(\frac{\hat{n}_{ry}}{n_y} \right) &= \frac{\tilde{w}_{ry}}{\tilde{w}_y} = \frac{\tilde{w}_{ry}}{\sum_{r \in \mathcal{P}} \tilde{w}_{ry}} \\ &= \frac{\sum_{s \in \mathcal{P}} \sum_{i=1}^n w_{rs} \mathbb{1}(\mathbf{x}_i \in Q_s) \mathbb{1}(y_i = y)}{\sum_{r \in \mathcal{P}} \sum_{s \in \mathcal{P}} \sum_{i=1}^n w_{rs} \mathbb{1}(\mathbf{x}_i \in Q_s) \mathbb{1}(y_i = y)}. \end{aligned}$$

As $n \rightarrow \infty$ and $h_n \rightarrow 0$, the estimated weights w_{rs} should satisfy the condition:

$$(13) \quad w_{rs} \rightarrow \begin{cases} 0, & \text{if } Q_r \neq Q_s \\ 1, & \text{if } Q_r = Q_s. \end{cases}$$

For simplicity, we will describe the estimation procedure for w_{rs} in the next sections. Note that if we satisfy Condition 13, then we have $\frac{\tilde{w}_{ry}}{\tilde{w}_y} \rightarrow \frac{n_{ry}}{n_y}$ as $n \rightarrow \infty$. Therefore, we modify Equation 5 as:

$$(14) \quad \tilde{f}_y(\mathbf{x}) = \frac{1}{\tilde{w}_y} \sum_{r \in \mathcal{P}} \tilde{w}_{ry} \mathcal{G}(\mathbf{x}; \hat{\mu}_r, \hat{\Sigma}_r) \mathbb{1}(r = \hat{r}_{\mathbf{x}}^*),$$

where $\hat{r}_{\mathbf{x}}^* = \arg\min_r \|\hat{\mu}_r - \mathbf{x}\|$. Now we use $\tilde{f}_y(\mathbf{x})$ estimated using (5) in Equation (6), (7) and (8), respectively. Below, we describe how we estimate w_{rs} for KDF and KDN.

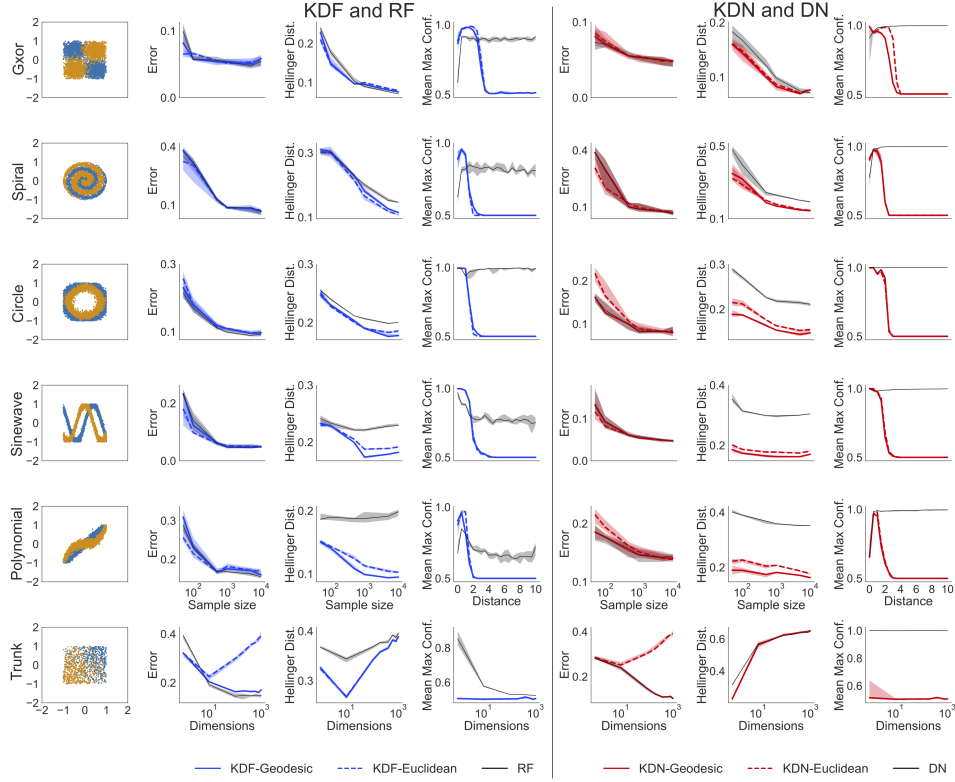


Figure 1: **Simulation datasets, Classification error, Hellinger distance from true posteriors, mean max confidence or posterior for the simulation experiments.** The simulation experiments were repeated 45 times. The median performance is shown as a dark curve with shaded region as error bars showing the 25-th and the 75-th percentile. KDF (Left block) and KDN (Right block) improve both in- and out-of-distribution calibration of their respective parent algorithms while maintaining nearly similar classification accuracy on the simulation datasets. For Trunk simulation sample size was fixed at 5000 for gradually higher number of dimensions and OOD test samples were sampled uniformly from a hyper-sphere with radius fixed at 20. Trunk simulation dataset is visualized for the first two dimensions.

5.3 Kernel Density Forest Consider T number of decision trees in a random forest trained on n i.i.d training samples $\{(\mathbf{x}_i, y_i)\}_{i=1}^n$. Each tree t partitions the feature space into p_t polytopes resulting in a set of polytopes: $\{\{Q_{t,r}\}_{r=1}^{p_t}\}_{t=1}^T$. The intersection of these polytopes gives a new set of polytopes $\{Q_r\}_{r=1}^p$ for the forest. For any point $\mathbf{x}_r \in Q_r$, we push every other sample point $\mathbf{x}_s \in Q_s$ down the trees. Now, we define the kernel $\mathcal{K}(r, s)$ as:

$$(15) \quad \mathcal{K}(r, s) = \frac{t_{rs}}{T},$$

where t_{rs} is the total number trees \mathbf{x}_r and \mathbf{x}_s end up in the same leaf node. Note that $0 \leq \mathcal{K}(r, s) \leq 1$. If the two samples end up in the same leaves in all the trees, they belong to the same polytope, i.e. $Q_r = Q_s$.

In short, $\mathcal{K}(r, s)$ is the fraction of total trees where the two samples follow the same path from the root to a leaf node. We exponentiate $\mathcal{K}(r, s)$ so that Condition 13 is satisfied:

$$(16) \quad w_{rs} = \mathcal{K}(r, s)^{k \log n}.$$

We choose k using grid search on a hold-out dataset.

5.4 Kernel Density Network Consider a fully connected ReLU-net trained on n iid training samples $\{(\mathbf{x}_i, y_i)\}_{i=1}^n$. We have the set of all nodes denoted by \mathcal{N}_l at a particular layer l . We can randomly pick a node $n_l \in \mathcal{N}_l$ at each layer l , and construct a sequence of nodes starting at the input layer

and ending at the output layer which we call an **activation path**: $m = \{n_l \in \mathcal{N}_l\}_{l=1}^L$. Note that there are $N = \prod_{l=1}^L |\mathcal{N}_l|$ possible activation paths for a sample in the ReLU-net. We index each path by a unique identifier number $z \in \mathbb{N}$ and construct a sequence of activation paths as: $\mathcal{M} = \{m_z\}_{z=1, \dots, N}$. Therefore, \mathcal{M} contains all possible activation pathways from the input to the output of the network.

While pushing a training sample \mathbf{x}_i through the network, we define the activation from a ReLU unit at any node as ‘1’ when it has non-negative input and ‘0’ otherwise. Therefore, the activation indicates on which side of the affine function at each node the sample falls. The activation for all nodes in an activation path m_z for a particular sample creates an **activation mode** $a_z \in \{0, 1\}^L$. If we evaluate the activation mode for all activation paths in \mathcal{M} while pushing a sample through the network, we get a sequence of activation modes: $\mathcal{A}_r = \{a_z^r\}_{z=1}^N$. Here r is the index of the polytope where the sample falls in.

If the two sequences of activation modes for two different training samples are identical, they belong to the same polytope. In other words, if $\mathcal{A}_r = \mathcal{A}_s$, then $Q_r = Q_s$. This statement holds because the above samples will lie on the same side of the affine function at each node in different layers of the network. Now, we define the kernel $\mathcal{K}(r, s)$ as:

$$(17) \quad \mathcal{K}(r, s) = \frac{\sum_{z=1}^N \mathbb{1}(a_z^r = a_z^s)}{N}.$$

Note that $0 \leq \mathcal{K}(r, s) \leq 1$. In short, $\mathcal{K}(r, s)$ is the fraction of total activation paths which are identically activated for two samples in two different polytopes r and s . We exponentiate the weights using Equation 16.

Pseudocodes outlining the two algorithms are provided in Appendix C.

5.5 Geodesic Distance Consider $\mathcal{P}_n = \{Q_1, Q_2, \dots, Q_p\}$ as a partition of \mathbb{R}^d given by a random forest or a ReLU-net after being trained on n training samples. We measure distance between two points $\mathbf{x} \in Q_r, \mathbf{x}' \in Q_s$ using the kernel introduced in Equation 15 and Equation 17 [22] and call it ‘Geodesic’ distance:

$$(18) \quad d(r, s) = -\mathcal{K}(r, s) + \frac{1}{2}(\mathcal{K}(r, r) + \mathcal{K}(s, s)) = 1 - \mathcal{K}(r, s)$$

Corollary 6. (\mathcal{P}_n, d) is a metric space.

Proof. See Appendix A.5 for the proof. ■

As d cannot distinguish between points within the same polytope, it has a resolution similar to the size of the polytope. For discriminating between two points within the same polytope, we fit a Gaussian kernel within the polytope (described above). As $h_n \rightarrow 0$, the resolution for Geodesic distance improves. Therefore, when we use geodesic distance in Equation 4, Theorem 1, 2 hold asymptotically for our approach. In the next section, we will empirically show that using Geodesic distance scales better with higher dimension compared to that of Euclidean distance.

6 Experimental Results We conduct several experiments on simulated, OpenML-CC18 [23]¹ and vision benchmark datasets to gain insights on the finite sample performance of KDF and KDN. The details of the simulation datasets and hyperparameters used for all the experiments are provided in Appendix B. For Trunk simulation dataset, we follow the simulation setup proposed by Trunk [24] which was designed to demonstrate ‘curse of dimensionality’. In the Trunk simulation, a binary class dataset is used where each class is sampled from a Gaussian distribution with higher dimensions having increasingly less discriminative information. We use both Euclidean and Geodesic distance in (4) on simulation

¹<https://www.openml.org/s/99>

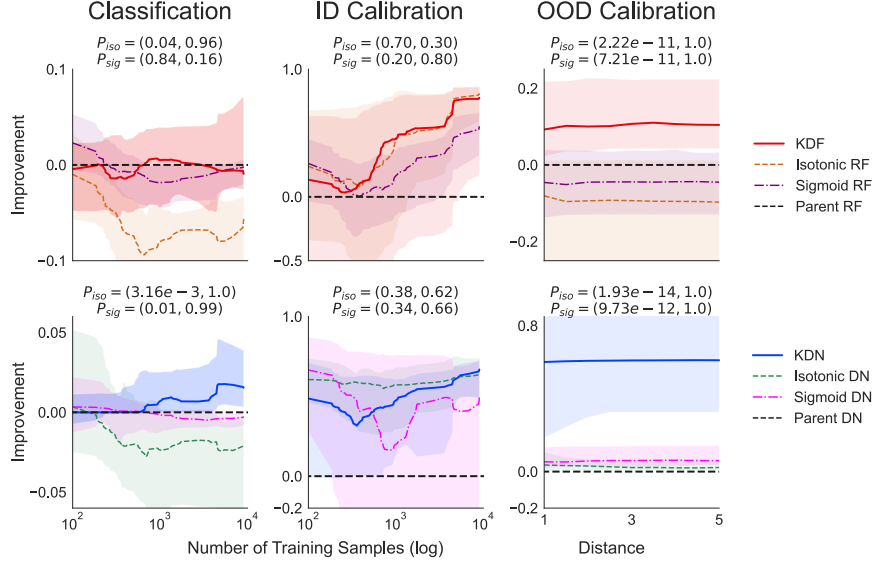


Figure 2: **Performance summary of KDF and KDN on OpenML-CC18 data suite.** The dark curve in the middle shows the median of performance on 45 datasets. The shaded region shows the error bar consisting of the 25-th and the 75-th percentile of the performance statistics. We conducted Wilcoxon rank-sum test using improvements in different datasets at the final sample size as test statistics. Each panel shows a p-value pair for each baseline approach where the first and second p-values correspond to testing whether baseline model performs worse and better than our approach respectively. **Left:** KDF and KDN maintains or improves performance of their parent algorithms for classification. **Middle:** KDF and KDN significantly improve the in-distribution calibration for random forest and ReLU-net. **Right:** Both of the proposed approaches yield highly calibrated confidence in the OOD region.

datasets and use only Geodesic distance for benchmark datasets. For the simulation setups, we use classification error, hellinger distance [25, 26] from the true class conditional posteriors and mean max confidence or posterior [4] as performance statistics. While measuring in-distribution calibration for the datasets in OpenML-CC18 data suite, as we do not know the true distribution, we used maximum calibration error as defined by Guo et al. [18] with a fixed bin number of $R = 15$ across all the datasets. Given n OOD samples, we define OOD calibration error (OCE) to measure OOD performance for the benchmark datasets as:

$$(19) \quad \text{OCE} = \frac{1}{n} \sum_{i=1}^n \left| \max_{y \in \mathcal{Y}} (\hat{P}_{Y|X}(y|\mathbf{x}_i)) - \max_{y \in \mathcal{Y}} (\hat{P}_Y(y)) \right|.$$

For the tabular and the vision datasets, we have used ID calibration approaches, such as ISOTONIC [15, 16] and SIGMOID [17] regression, as baselines. Additionally, for the vision benchmark dataset, we provide results with an OOD calibration approach ACET [4], and report traditionally used OOD detection statistics such as area under curve (AUROC) and false positive rate at 95% precision (FPR@95). For each approach, 90% of the training data was used to fit the model and the rest of the data was used to calibrate the model.

Table 1: Performance Summary on different Vision Datasets for Different Algorithms When Trained on CIFAR-10

Dataset	Statistics	Parent	KDN	ISOTONIC	SIGMOID	ACET
CIFAR-10	Accuracy(%)	83.70	83.60	83.68	83.70	80.17
	MCE	0.13	0.02	0.02	0.04	0.17
CIFAR-100	OCE	0.78	0.52	0.53	0.69	0.83
	AUROC (FPR@95)	0.78(0.83)	0.69(0.74)	0.79(0.77)	0.67(0.83)	0.72(0.86)
SVHN	OCE	0.73	0.52	0.43	0.66	0.78
	AUROC (FPR@95)	0.84(0.74)	0.86(0.81)	0.87(0.59)	0.67(0.75)	0.83(0.74)
Noise	OCE	0.84	0.00	0.68	0.72	0.00
	AUROC (FPR@95)	0.71(0.92)	0.98(0.0)	0.71(0.96)	0.40(0.92)	1.00(0.0)

6.1 Simulation Study Figure 1 leftmost column shows 10000 training samples with 5000 samples per class sampled within the region $[-1, 1] \times [-1, 1]$ from the six simulation setups described in Appendix B. Therefore, the empty annular region between $[-1, 1] \times [-1, 1]$ and $[-2, 2] \times [-2, 2]$ is the low density or OOD region in Figure 1. Figure 1 quantifies the performance of the algorithms which are visually represented in Appendix Figure 3. KDF and KDN maintain similar classification accuracy to those of their parent algorithms. We measure hellinger distance from the true distribution for increasing training sample size within $[-1, 1] \times [-1, 1]$ region as a statistics for in-distribution calibration. Column 3 of left and Column 2 of right block in Figure 1 show KDF and KDN are better at estimating the high density region of training distribution compared to their parent methods. In all of the simulations, using geodesic distance measure results in better performance compared to those while using Euclidean distance. For measuring OOD performance, we keep the training sample size fixed at 1000 and normalize the training data by the maximum of their l_2 norm so that the training data is confined within a unit circle. For inference, we sample 1000 inference points uniformly from a circle where the circles have increasing radius and plot mean max posterior for increasing distance from the origin. Therefore, for distance up to 1 we have in-distribution samples and distances farther than 1 can be considered as OOD region. As shown in Column 3 of Figure 1, mean max posteriors or confidence for KDF and KDN converge to the maximum of the class priors, i.e., 0.5 as we go farther away from the training data origin.

Row 6 of Figure 1 shows KDF-Geodesic and KDN-Geodesic scale better with higher dimensions compared to their Euclidean counterpart algorithms respectively.

6.2 OpenML-CC18 Data Study We used OpenML-CC18 data suite for tabular benchmark dataset study. We exclude any dataset which contains categorical features or NaN values² and conduct our experiments on 45 datasets with varying dimensions and sample sizes. For the OOD experiments, we follow a similar setup as that of the simulation data. We normalize the training data by their maximum l_2 norm and sample 1000 testing samples uniformly from each hypersphere where the hyperspheres have increasing radius starting from 1 to 5. For each dataset, we measure improvement with respect to the parent algorithm as:

$$(20) \quad \frac{\mathcal{E}_p - \mathcal{E}_M}{\mathcal{E}_p},$$

where \mathcal{E}_p =classification error, MCE or OCE for the parent algorithm and \mathcal{E}_M represents the performance of the approach in consideration. Note that positive improvement implies the corresponding approach performs better than the parent approach. We report the median of improvement on different datasets along with the error bar in Figure 2. The extended results for each dataset is shown separately in the appendix. Figure 2 left column shows on average KDF and KDN has nearly similar or better classification accuracy to their respective parent algorithm whereas ISOTONIC and SIGMOID regression have lower classification accuracy most of the cases. However, according to Figure 2 middle column, KDF and KDN have similar in-distribution calibration performance to the other baseline approaches. Most interestingly, Figure 2 right column shows that KDN and KDF improves OOD calibration of their respective parent algorithms by a huge margin while the baseline approaches completely fails to address the OOD calibration problem.

6.3 Vision Benchmark Datasets Study For vision experiments, we trained a RESNET-20 model on CIFAR-10 dataset and calibrated it using different ID and OOD calibration approaches. As shown in Table 1, ID calibration, i.e., ISOTONIC and SIGMOID regression have relatively better calibration for near OOD datasets like CIFAR-100 and SVHN compared to OOD calibration approach ACET. However, ID calibration approaches have worse far OOD (noise) performance compared to ACET. Interestingly,

²We also excluded the dataset with dataset id 23517 as we could not achieve better than chance accuracy using RF and DN on that dataset.

KDN achieves a compromise between ID and OOD calibration approaches by treating the calibration problem as a continuum rather than two separate problems.

As the results suggest, KDN effectively solves ID and far OOD calibration problem. However, for improving near OOD performance, it requires further work. For example, as shown by Fort et al. [27], near OOD performance for KDN may be improved further by using a few known outliers. Another possible improvement can be achieved by using other kernels which can capture local correlation between the samples within a polytope better than the Gaussian kernel. However, for keeping the focus of the paper concise, we will pursue near OOD calibration in our future work.

7 Discussion In this paper, we convert deep discriminative network to kernel density network by replacing the affine function over the polytopes in the discriminative networks with a Gaussian kernel. This replacement of affine function results in better in- and out-of-distribution calibration for our proposed approaches while having classification accuracy similar to or better than the parent algorithm. Theoretically, we show under certain conditions our approaches asymptotically converge to the true training distribution and this establishes confidence calibration for learning algorithms in in- and out-of-distribution regions as a continuum rather than two different problems.

Acknowledgements The authors thank the support of the NSF-Simons Research Collaborations on the Mathematical and Scientific Foundations of Deep Learning (NSF grant 2031985) and THEORINET. This work is graciously supported by the Defense Advanced Research Projects Agency (DARPA) Life-long Learning Machines program through contracts FA8650-18-2-7834 and HR0011-18-2-0025. Research was partially supported by funding from Microsoft Research and the Kavli Neuroscience Discovery Institute.

References

- [1] Chuan Guo, Geoff Pleiss, Yu Sun, and Kilian Q. Weinberger. On calibration of modern neural networks. In Doina Precup and Yee Whye Teh, editors, *Proceedings of the 34th International Conference on Machine Learning*, volume 70 of *Proceedings of Machine Learning Research*, pages 1321–1330. PMLR, 06–11 Aug 2017.
- [2] Agustinus Kristiadi, Matthias Hein, and Philipp Hennig. Being bayesian, even just a bit, fixes overconfidence in ReLU networks. In Hal Daumé III and Aarti Singh, editors, *Proceedings of the 37th International Conference on Machine Learning*, volume 119 of *Proceedings of Machine Learning Research*, pages 5436–5446. PMLR, 13–18 Jul 2020.
- [3] Haoyin Xu, Kaleab A. Kinfu, Will LeVine, Sambit Panda, Jayanta Dey, Michael Ainsworth, Yu-Chung Peng, Madi Kusmanov, Florian Engert, Christopher M. White, Joshua T. Vogelstein, and Carey E. Priebe. When are Deep Networks really better than Decision Forests at small sample sizes, and how? *arXiv preprint arXiv:2108.13637*, 2021.
- [4] Matthias Hein, Maksym Andriushchenko, and Julian Bitterwolf. Why relu networks yield high-confidence predictions far away from the training data and how to mitigate the problem. In *Proceedings of the IEEE/CVF Conference on Computer Vision and Pattern Recognition*, pages 41–50, 2019.
- [5] Alexander Meinke, Julian Bitterwolf, and Matthias Hein. Provably robust detection of out-of-distribution data (almost) for free. *arXiv preprint arXiv:2106.04260*, 2021.
- [6] Shiyu Liang, Yixuan Li, and Rayadurgam Srikant. Enhancing the reliability of out-of-distribution image detection in neural networks. *arXiv preprint arXiv:1706.02690*, 2017.
- [7] Jay Nandy, Wynne Hsu, and Mong Li Lee. Towards maximizing the representation gap between in-domain & out-of-distribution examples. *Advances in Neural Information Processing Systems*, 33:9239–9250, 2020.
- [8] Weitao Wan, Yuanyi Zhong, Tianpeng Li, and Jiansheng Chen. Rethinking feature distribution for

- loss functions in image classification. In *Proceedings of the IEEE conference on computer vision and pattern recognition*, pages 9117–9126, 2018.
- [9] Terrance DeVries and Graham W Taylor. Learning confidence for out-of-distribution detection in neural networks. *arXiv preprint arXiv:1802.04865*, 2018.
 - [10] Dan Hendrycks, Mantas Mazeika, and Thomas Dietterich. Deep anomaly detection with outlier exposure. *arXiv preprint arXiv:1812.04606*, 2018.
 - [11] Jie Ren, Peter J Liu, Emily Fertig, Jasper Snoek, Ryan Poplin, Mark Depristo, Joshua Dillon, and Balaji Lakshminarayanan. Likelihood ratios for out-of-distribution detection. *Advances in neural information processing systems*, 32, 2019.
 - [12] Diederik P Kingma, Max Welling, et al. An introduction to variational autoencoders. *Foundations and Trends® in Machine Learning*, 12(4):307–392, 2019.
 - [13] Ian Goodfellow, Jean Pouget-Abadie, Mehdi Mirza, Bing Xu, David Warde-Farley, Sherjil Ozair, Aaron Courville, and Yoshua Bengio. Generative adversarial networks. *Communications of the ACM*, 63(11):139–144, 2020.
 - [14] Eric Nalisnick, Akihiro Matsukawa, Yee Whye Teh, Dilan Gorur, and Balaji Lakshminarayanan. Do deep generative models know what they don’t know? *arXiv preprint arXiv:1810.09136*, 2018.
 - [15] Bianca Zadrozny and Charles Elkan. Obtaining calibrated probability estimates from decision trees and naive bayesian classifiers. In *icml*, volume 1, pages 609–616, 2001.
 - [16] R Caruana. Predicting good probabilities with supervised learning. In *Proceedings of NIPS 2004 Workshop on Calibration and Probabilistic Prediction in Supervised Learning*, 2004.
 - [17] John Platt et al. Probabilistic outputs for support vector machines and comparisons to regularized likelihood methods. *Advances in large margin classifiers*, 10(3):61–74, 1999.
 - [18] Chuan Guo, Geoff Pleiss, Yu Sun, and Kilian Q Weinberger. On calibration of modern neural networks. In *International conference on machine learning*, pages 1321–1330. PMLR, 2017.
 - [19] Richard Guo, Ronak Mehta, Jesus Arroyo, Hayden Helm, Cencheng Shen, and Joshua T Vogelstein. Estimating information-theoretic quantities with uncertainty forests. *arXiv*, pages arXiv–1907, 2019.
 - [20] Meelis Kull, Miquel Perello Nieto, Markus Kängsepp, Telmo Silva Filho, Hao Song, and Peter Flach. Beyond temperature scaling: Obtaining well-calibrated multi-class probabilities with dirichlet calibration. *Advances in neural information processing systems*, 32, 2019.
 - [21] Haoyin Xu, Kaleab A Kinfu, Will LeVine, Sambit Panda, Jayanta Dey, Michael Ainsworth, Yu-Chung Peng, Madi Kusmanov, Florian Engert, Christopher M White, et al. When are deep networks really better than decision forests at small sample sizes, and how? *arXiv preprint arXiv:2108.13637*, 2021.
 - [22] Bernhard Schölkopf. The kernel trick for distances. *Advances in neural information processing systems*, 13, 2000.
 - [23] Bernd Bischl, Giuseppe Casalicchio, Matthias Feurer, Pieter Gijsbers, Frank Hutter, Michel Lang, Rafael G Mantovani, Jan N van Rijn, and Joaquin Vanschoren. Openml benchmarking suites. *arXiv preprint arXiv:1708.03731*, 2017.
 - [24] Gerard V Trunk. A problem of dimensionality: A simple example. *IEEE Transactions on pattern analysis and machine intelligence*, (3):306–307, 1979.
 - [25] Thomas Kailath. The divergence and bhattacharyya distance measures in signal selection. *IEEE transactions on communication technology*, 15(1):52–60, 1967.
 - [26] C Radhakrishna Rao. A review of canonical coordinates and an alternative to correspondence analysis using hellinger distance. *Qüestió: quaderns d’estadística i investigació operativa*, 1995.
 - [27] Stanislav Fort, Jie Ren, and Balaji Lakshminarayanan. Exploring the limits of out-of-distribution detection. *Advances in Neural Information Processing Systems*, 34:7068–7081, 2021.
 - [28] Ronan Perry, Ronak Mehta, Richard Guo, Eva Yezerets, Jesús Arroyo, Mike Powell, Hayden Helm, Cencheng Shen, and Joshua T Vogelstein. Random forests for adaptive nearest neighbor estima-

- tion of information-theoretic quantities. [arXiv preprint arXiv:1907.00325](#), 2019.
- [29] Susan Athey, Julie Tibshirani, and Stefan Wager. Generalized random forests. 2019.
- [30] Kurt Hornik, Maxwell Stinchcombe, and Halbert White. Multilayer feedforward networks are universal approximators. [Neural networks](#), 2(5):359–366, 1989.

Appendix A. Proofs.

A.1 Proof of Theorem 1 Consider the density estimator for the samples populating the polytopes \hat{f} . Let n be the total number of samples and n_r be the number of data points within polytope Q_r . As stated in the theorem statement, we make the following assumptions:

1. The polytope bandwidth $h_n \rightarrow 0$ as $n \rightarrow \infty$.
2. n grows faster than the shrinkage of h_n , i.e., $n \cdot h_n \rightarrow \infty$ as $h_n \rightarrow 0$ in probability.

For simplicity, we first explore the one-dimensional distribution. The derivation can be readily extended to multi-dimensional scenarios. We consider any Gaussian kernel $\mathcal{G}'()$ with parameters chosen independently of the data satisfying two conditions. In lemma 7 and 8, we will show that the aforementioned class of estimators is consistent. The conditions for choosing the Gaussian kernel parameters are:

1. The center of the kernel can be any point z_r within the polytope Q_r as $n \rightarrow \infty$,
2. The kernel bandwidth σ_r is any non-negative number always bounded by the polytope bandwidth h_n as $n \rightarrow \infty$, i.e., $\sigma_r = C_r h_n$, where $0 < C_r < 1$.

Now the class conditional density estimate at a point x can be written as:

$$(21) \quad \hat{f}(x) = \frac{1}{n} \sum_{r \in \mathcal{P}} n_r \mathcal{G}'(x; \mu_r, \Sigma_r) \mathbb{1}(r = r_x^*).$$

Lemma 7. *The class of estimators in (21) is an asymptotically unbiased class of estimators of the true density f .*

Proof. The polytope sample counts n_r can be considered as binomially distributed: $n_r \sim B(n, P_r)$, where $P_r = \int_{Q_r} dF$ is the probability of finding a training sample within the polytope r and F is the cumulative density function associated with the density f . This allows us to write: $\mathbb{E}[n_r] = n P_r$. Using the mean value theorem, we have that $P_r = h_n f(q_r)$, for some $q_r \in Q_r$. Note that, if we consider the multi-dimensional scenario for the mean value theorem here, the proof can be easily generalized for multi-dimensional case.

Now consider the expectation of \hat{f} with respect to the training distribution:

$$(22) \quad \mathbb{E}[\hat{f}(x)] = \sum_{r \in \mathcal{P}} \frac{n P_r \mathcal{G}'(x; \mu_r, \Sigma_r) \mathbb{1}(r = r_x^*)}{n}$$

$$(23) \quad = \sum_{r \in \mathcal{P}} h_n f(q_r) \mathcal{G}'(x; \mu_r, \Sigma_r) \mathbb{1}(r = r_x^*).$$

Note that we are given the partitions of the feature space and we choose Gaussian parameters such that they are independent of the training data. Now, as $n \rightarrow \infty$, $h_n \rightarrow 0$, and h_n can be considered an infinitesimal measure dz_r . Furthermore, as the bandwidth of the Gaussian is limited by the polytope bandwidth and the area under the Gaussian is 1, the kernel summation $\sum_{r \in \mathcal{P}} \mathcal{G}'(x, \mu_r, \Sigma_r) \mathbb{1}(r = r_x^*)$ becomes a dirac delta function evaluated at x as $h_n \rightarrow 0$. Therefore, in the limiting conditions, $\sum_{r \in \mathcal{P}} \mathcal{G}'(x, \mu_r, \Sigma_r) \mathbb{1}(r = r_x^*) \rightarrow \delta(z_r - x)$ and $f(q_r) \rightarrow f(z_r)$. Here z_r is a point such that $z_r \in Q_r$ for all n and $\sigma_r < h_n$. Therefore, there exists a small positive number ϵ for which we can rewrite 23 as:

$$(24) \quad \begin{aligned} \mathbb{E}[\hat{f}(x)] &= \int_{x-\epsilon}^{x+\epsilon} f(z_r) \delta(z_r - x) dz_r \\ &= f(x) \end{aligned}$$

Therefore, $\hat{f}(x)$ is an asymptotically unbiased estimator of $f(x)$. ■

Lemma 8. The variance of the class of estimators in (21) asymptotically goes to 0.

Proof. For binomially distributed samples n_r , we can write, $\mathbb{V}ar[n_r] = nP_r(1 - P_r)$. Therefore, we can estimate the variance of $\hat{f}(x)$ as:

$$\begin{aligned}
 \mathbb{V}ar[\hat{f}(x)] &= \sum_{r \in \mathcal{P}} \frac{nP_r(1 - P_r)}{n^2} \{\mathcal{G}'(x; \mu_r, \Sigma_r) \mathbb{1}(r = r_x^*)\}^2 \\
 &= \frac{h_n f(z_{r_x^*})(1 - h_n f(z_{r_x^*}))}{n} \left\{ \frac{1}{\sqrt{2\pi}\sigma_{r_x^*}} \exp\left(-\frac{(x - \mu_{r_x^*})^2}{2\sigma_{r_x^*}^2}\right) \right\}^2 \\
 &= \frac{h_n f(z_{r_x^*})(1 - h_n f(z_{r_x^*}))}{nC_{r_x^*}^2 h_n^2} \left\{ \frac{1}{\sqrt{2\pi}} \exp\left(-\frac{(x - \mu_{r_x^*})^2}{2\sigma_{r_x^*}^2}\right) \right\}^2 \\
 &\leq \frac{f(z_{r_x^*})(1 - h_n f(z_{r_x^*}))}{2\pi C_{r_x^*}^2 (nh_n)}
 \end{aligned}
 \tag{25}$$

Equation 25 offers several interesting insights:

1. As $h_n \rightarrow 0$, $z_{r_x^*} \rightarrow x$ and $f(z_{r_x^*})(1 - h_n f(z_{r_x^*})) \rightarrow f(x)$. Therefore, the variance becomes directly dependent on $f(x)$. There is more variability at regions with higher density.

2. The variance is also higher if $C_{r_x^*}^2 \ll 1$. Therefore, $C_{r_x^*}$ should be as close to 1 as possible and nh_n should be as high as possible for lower variance. Moreover, variance can be reduced at the expense of higher bias with $C_{r_x^*} > 1$. Most importantly note that, the effect of $C_{r_x^*}$ cancels out in the numerator and the denominator while estimating the posteriors in Equation 7.

3. As $h_n \rightarrow 0$ the estimation becomes unbiased (see Equation 23), but the estimation variance becomes unbounded. Therefore, for bounded and decreasing variance the condition $nh_n \rightarrow \infty$ is necessary. ■

Lemma 7 and 8 together completes the proof of Theorem 1.

A.2 Proof of Theorem 2 We first expand $\hat{g}_y(\mathbf{x})$:

$$\begin{aligned}
 \hat{g}_y(\mathbf{x}) &= \frac{\hat{f}_y(\mathbf{x}) \hat{P}_Y(y)}{\sum_{k=1}^K \hat{f}_k(\mathbf{x}) \hat{P}_Y(k)} \\
 &= \frac{\hat{f}_y(\mathbf{x}) \hat{P}_Y(y) + \frac{b}{\log(n)} \hat{P}_Y(y)}{\sum_{k=1}^K (\hat{f}_k(\mathbf{x}) \hat{P}_Y(k) + \frac{b}{\log(n)} \hat{P}_Y(k))}
 \end{aligned}$$

As the inference point \mathbf{x} becomes more distant from training samples (and more distant from all of the Gaussian centers), we have that $\mathcal{G}(\mathbf{x}, \hat{\mu}_r, \hat{\Sigma}_r)$ becomes smaller. Thus, $\forall y, \tilde{f}_y(\mathbf{x})$ shrinks. More formally, $\forall y$,

$$\lim_{d_{\mathbf{x}} \rightarrow \infty} \tilde{f}_y(\mathbf{x}) = 0$$

We can use this result to then examine the limiting behavior of our posteriors as the inference point \mathbf{x} becomes more distant from the training data:

$$\begin{aligned}
 \lim_{d_{\mathbf{x}} \rightarrow \infty} \hat{g}_y(\mathbf{x}) &= \lim_{d_{\mathbf{x}} \rightarrow \infty} \frac{\tilde{f}_y(\mathbf{x}) \hat{P}_Y(y) + \frac{b}{\log(n)} \hat{P}_Y(y)}{\sum_{k=1}^K (\tilde{f}_k(\mathbf{x}) \hat{P}_Y(k) + \frac{b}{\log(n)} \hat{P}_Y(k))} \\
 &= \frac{(\lim_{d_{\mathbf{x}} \rightarrow \infty} \tilde{f}_y(\mathbf{x})) \hat{P}_Y(y) + \frac{b}{\log(n)} \hat{P}_Y(y)}{\sum_{k=1}^K (\lim_{d_{\mathbf{x}} \rightarrow \infty} \tilde{f}_k(\mathbf{x}) \hat{P}_Y(k) + \frac{b}{\log(n)} \hat{P}_Y(k))} \\
 &= \frac{\hat{P}_Y(y)}{\sum_{k=1}^K \hat{P}_Y(k)} \\
 &= \hat{P}_Y(y)
 \end{aligned}$$

A.3 Proof of Corollary 4 Consider a class of random forest algorithms and a training distribution which satisfies all the conditions mentioned in Perry et al. [28], Athey et al. [29]. The above class of algorithms partitions the feature space so that as $n \rightarrow \infty$, the average polytope bandwidth $h_n \rightarrow 0$ and $nh_n \rightarrow \infty$.

A.4 Proof of Corollary 5 Consider a training distribution that satisfies all the conditions mentioned in [28, 29]. Using the universal approximation theorems for neural networks [30], we can say the number of parameters for deep-net should increase as $n \rightarrow \infty$ for an unbiased estimation of the posteriors. In other words, the number of affine function should increase resulting in a finer partition of the feature space, i.e., $h_n \rightarrow 0$ and $nh_n \rightarrow \infty$ for the polytopes.

A.5 Proof of Corollary 6 For proving that d is a valid distance metric for \mathcal{P}_n , we need to prove the following four statements:

1. $d(r, s) = 0$ when $r = s$.

Proof: By definition, $\mathcal{K}(r, s) = 1$ and $d(r, s) = 0$ when $r = s$.

2. $d(r, s) > 0$ when $r \neq s$.

Proof: By definition, $0 \leq \mathcal{K}(r, s) < 1$ and $d(r, s) > 0$ for $r \neq s$.

3. d is symmetric, i.e., $d(r, s) = d(s, r)$.

Proof: By definition, $\mathcal{K}(r, s) = \mathcal{K}(s, r)$ which implies $d(r, s) = d(s, r)$.

4. d follows the triangle inequality, i.e., for any three polytopes $Q_r, Q_s, Q_t \in \mathcal{P}_n$: $d(r, t) \leq d(r, s) + d(s, t)$.

Proof: Let \mathcal{A}_r denote the set of activation modes in a ReLU-net and the set of leaf nodes in a random forest for a particular polytope r . N is the total number of possible activation paths in a ReLU-net or total trees in a random forest. We can write:

$$\begin{aligned}
 (26) \quad N &\geq n((\mathcal{A}_r \cap \mathcal{A}_s) \cup (\mathcal{A}_s \cap \mathcal{A}_t)) \\
 &= n(\mathcal{A}_r \cap \mathcal{A}_s) + n(\mathcal{A}_s \cap \mathcal{A}_t) - n(\mathcal{A}_r \cap \mathcal{A}_s \cap \mathcal{A}_t) \\
 &\geq n(\mathcal{A}_r \cap \mathcal{A}_s) + n(\mathcal{A}_s \cap \mathcal{A}_t) - n(\mathcal{A}_r \cap \mathcal{A}_t)
 \end{aligned}$$

Rearranging the above equation, we get:

$$\begin{aligned}
 N - n(\mathcal{A}_r \cap \mathcal{A}_t) &\leq N - n(\mathcal{A}_r \cap \mathcal{A}_s) + N - n(\mathcal{A}_s \cap \mathcal{A}_t) \\
 \implies 1 - \frac{n(\mathcal{A}_r \cap \mathcal{A}_t)}{N} &\leq 1 - \frac{n(\mathcal{A}_r \cap \mathcal{A}_s)}{N} + 1 \\
 &\quad - \frac{n(\mathcal{A}_s \cap \mathcal{A}_t)}{N} \\
 (27) \quad \implies d(r, t) &\leq d(r, s) + d(s, t)
 \end{aligned}$$

Appendix B. Simulations.

We construct six types of binary class simulations:

- *Gaussian XOR* is a two-class classification problem with equal class priors. Conditioned on being in class 0, a sample is drawn from a mixture of two Gaussians with means $\pm[0.5, -0.5]^\top$ and standard deviations of 0.25. Conditioned on being in class 1, a sample is drawn from a mixture of two Gaussians with means $\pm[0.5, -0.5]^\top$ and standard deviations of 0.25.
- *Spiral* is a two-class classification problem with the following data distributions: let K be the number of classes and $S \sim \text{multinomial}(\frac{1}{K}\mathbf{1}_K, n)$. Conditioned on S , each feature vector is parameterized by two variables, the radius r and an angle θ . For each sample, r is sampled uniformly in $[0, 1]$. Conditioned on a particular class, the angles are evenly spaced between $\frac{4\pi(k-1)t_K}{K}$ and $\frac{4\pi(k)t_K}{K}$, where t_K controls the number of turns in the spiral. To inject noise along

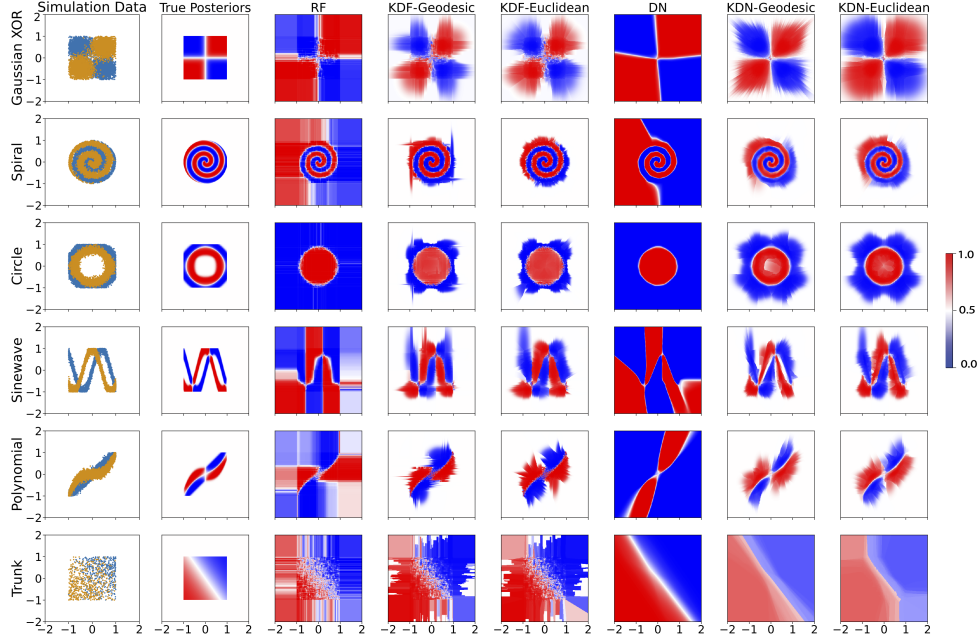


Figure 3: **Visualization of true and estimated posteriors for class 0 from five binary class simulation experiments.** *Column 1:* 10,000 training points with 5,000 samples per class sampled from 6 different simulation setups for binary class classification. Trunk simulation is shown for two dimensional case. The class labels are indicated by yellow and blue colors. *Column 2-8:* True and estimated class conditional posteriors from different approaches. The posteriors estimated from KDN and KDF are better calibrated for both in- and out-of-distribution regions compared to those of their parent algorithms.

the spirals, we add Gaussian noise to the evenly spaced angles $\theta' : \theta = \theta' + \mathcal{N}(0, 0.09)$. The observed feature vector is then $(r \cos(\theta), r \sin(\theta))$.

- *Circle* is a two-class classification problem with equal class priors. Conditioned on being in class 0, a sample is drawn from a circle centered at $(0, 0)$ with a radius of $r = 0.75$. Conditioned on being in class 1, a sample is drawn from a circle centered at $(0, 0)$ with a radius of $r = 1$, which is cut off by the region bounds. To inject noise along the circles, we add Gaussian noise to the circle radii $r' : r = r' + \mathcal{N}(0, 0.01)$.
- *Sinewave* is a two-class classification problem based on sine waves. Conditioned on being in class 0, a sample is drawn from the distribution $y = \cos(\pi x)$. Conditioned on being in class 1, a sample is drawn from the distribution $y = \sin(\pi x)$. We inject Gaussian noise to the sine wave heights $y' : y = y' + \mathcal{N}(0, 0.01)$.
- *Polynomial* is a two-class classification problem with the following data distributions: $y = x^a$. Conditioned on being in class 0, a sample is drawn from the distribution $y = x^1$. Conditioned on being in class 1, a sample is drawn from the distribution $y = x^3$. Gaussian noise is added to variables $y' : y = y' + \mathcal{N}(0, 0.01)$.
- *Trunk* is a two-class classification problem with gradually increasing dimension and equal class priors. The class conditional probabilities are Gaussian:

$$\begin{aligned} P(X|Y = 0) &= \mathcal{G}(\mu_1, I), \\ P(X|Y = 1) &= \mathcal{G}(\mu_2, I), \end{aligned}$$

where $\mu_1 = \mu, \mu_2 = -\mu$, μ is a d dimensional vector whose i -th component is $(\frac{1}{i})^{1/2}$ and I is d dimensional identity matrix.

Appendix C. Pseudocodes. We provide the pseudocode for our proposed algorithms in Algorithm 1, 2 and 3.

Table 2: Hyperparameters for RF and KDF.

Hyperparameters	Value
n_estimators	500
max_depth	∞
min_samples_leaf	1
b (bias)	$\exp(-10^{\sqrt{d}})$
λ	1×10^{-6}

Table 3: Hyperparameters for ReLU-net and KDN.

Hyperparameters	Value
number of hidden layers	4
nodes per hidden layer	1000
optimizer	Adam
learning rate	3×10^{-4}
b (bias)	$\exp(-10^{\sqrt{d}})$
λ	1×10^{-6}

Algorithm 1 Fit a KGX model.**Input:**

- (1) θ ▷ Parent learner (random forest or deep network model)
(2) $\mathcal{D}_n = (\mathbf{X}, \mathbf{y}) \in \mathbb{R}^{n \times d} \times \{1, \dots, K\}^n$ ▷ Training data

Output: \mathcal{G} ▷ a KGX model

```

1: function KGX.FIT( $\theta, \mathbf{X}, \mathbf{y}$ )
2:   for  $i = 1, \dots, n$  do ▷ Iterate over the dataset to calculate the weights
3:     for  $j = 1, \dots, n$  do
4:        $w_{ij} \leftarrow \text{COMPUTEWEIGHTS}(\mathbf{x}_i, \mathbf{x}_j, \theta)$ 
5:     end for
6:   end for
7:
8:
9:    $\{Q_r\}_{r=1}^{\tilde{p}} \leftarrow \text{GETPOLYTOPES}(\mathbf{w})$  ▷ Identify the polytopes by clustering the samples with similar weight
10:
11:    $\mathcal{G}.\{\tilde{w}_k\}_{k=1}^K \leftarrow 0$  ▷ Initialize the counts for each class
12:   for  $r = 1, \dots, \tilde{p}$  do ▷ Iterate over each polytope
13:     for  $k = 1, \dots, K$  do
14:        $\mathcal{G}.\tilde{w}_{rk} \leftarrow \text{COUNTWEIGHTS}(\{\mathbf{w}_{rs}\}_{s=1}^{\tilde{p}}, k)$  ▷  $w_{rk}$  is the number of weighted input samples in  $Q_r$  with label  $k$ 
15:        $\mathcal{G}.\tilde{w}_k \leftarrow \mathcal{G}.\tilde{w}_k + \mathcal{G}.\tilde{w}_{rk}$  ▷ Update the total count for each class
16:     end for
17:      $\mathcal{G}.\hat{\mu}_r, \mathcal{G}.\hat{\Sigma}_r \leftarrow \text{ESTIMATEPARAMETERS}(\mathbf{X}, \{\mathbf{w}_{rs}\}_{s=1}^{\tilde{p}})$  ▷ Fit Gaussians using weighted MLE
18:   end for
19:   return  $\mathcal{G}$ 
20: end function

```

Appendix D. Hardware and Software Configurations.

- Operating System: Linux (ubuntu 20.04), macOS (Ventura 13.2.1)

Algorithm 2 Computing weights in KDF

Input:

- (1) $\mathbf{x}_i, \mathbf{x}_j \in \mathbb{R}^{1 \times d}$ ▷ two input samples to be weighted
(2) θ ▷ parent random forest with T trees

Output: $w_{ij} \in [0, 1]$ ▷ compute similarity between i and j -th samples.

```
1: function COMPUTEWEIGHTS( $\mathbf{x}_i, \mathbf{x}_j, \theta$ )  
2:    $\mathcal{I}_i \leftarrow \text{PUSHDOWNTREES}(\mathbf{x}_i, \theta)$  ▷ push  $\mathbf{x}_i$  down  $T$  trees and get the leaf numbers it end up in.  
3:    $\mathcal{I}_j \leftarrow \text{PUSHDOWNTREES}(\mathbf{x}_j, \theta)$  ▷ push  $\mathbf{x}_j$  down  $T$  trees and get the leaf numbers it end up in.  
4:    $l \leftarrow \text{COUNTMATCHES}(\mathcal{I}_i, \mathcal{I}_j)$  ▷ count the number of times the samples end up in the same leaf  
5:    $w_{ij} \leftarrow \frac{l}{T}$   
6:   return  $w_{ij}$   
7: end function
```

Algorithm 3 Computing weights in KDN

Input:

- (1) $\mathbf{x}_i, \mathbf{x}_j \in \mathbb{R}^{1 \times d}$ ▷ two input samples to be weighted
(2) θ ▷ parent deep-net model

Output: $w_{ij} \in [0, 1]$ ▷ compute similarity between i and j -th samples.

```
1: function COMPUTEWEIGHTS( $\mathbf{x}_i, \mathbf{x}_j, \theta$ )  
2:    $\mathcal{A}_i \leftarrow \text{PUSHDOWNNETWORK}(\mathbf{x}_i, \theta)$  ▷ get activation modes  $\mathcal{A}_i$   
3:    $\mathcal{A}_j \leftarrow \text{PUSHDOWNNETWORK}(\mathbf{x}_j, \theta)$  ▷ get activation modes  $\mathcal{A}_j$   
4:    $l \leftarrow \text{COUNTMATCHES}(\mathcal{A}_i, \mathcal{A}_j)$  ▷ count the number of times the two samples activate the  
activation paths in a similar way  
5:    $w_{ij} \leftarrow \frac{l}{N}$  ▷  $N$  is the total number of activation paths  
6:   return  $w_{ij}$   
7: end function
```

- VM Size: Azure Standard D96as v4 (96 vcpus, 384 GiB memory)
- GPU: Apple M1 Max
- Software: Python 3.8, scikit-learn $\geq 0.22.0$, tensorflow-macos ≤ 2.9 , tensorflow-metal $\leq 0.5.0$.

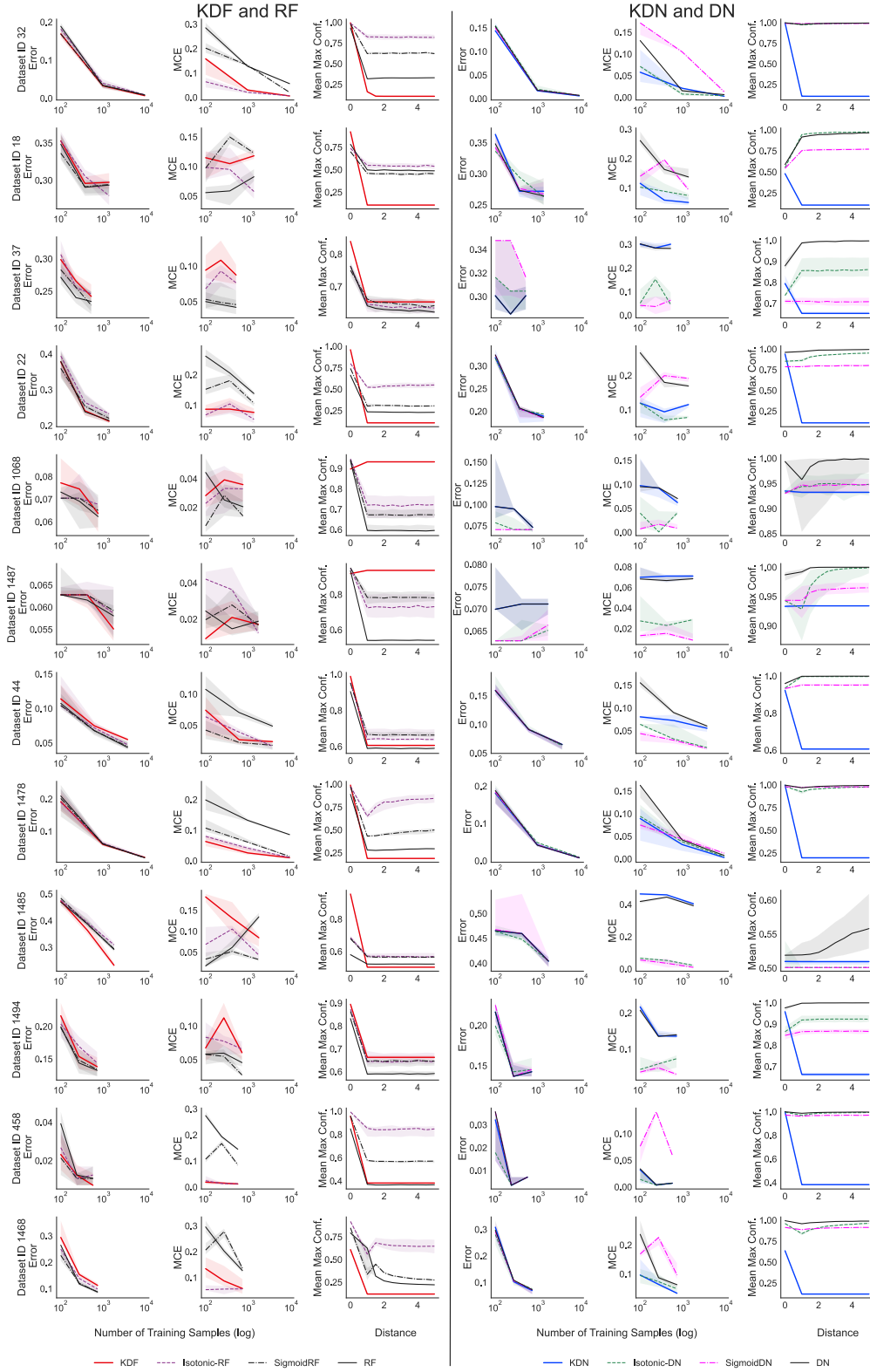


Figure 4: **Extended results on OpenML-CC18 datasets.** *Left:* Performance (classification error, MCE and mean max confidence) of KDF on different Openml-CC18 datasets. *Right:* Performance (classification error, MCE and mean max confidence) of KDN on different Openml-CC18 datasets.

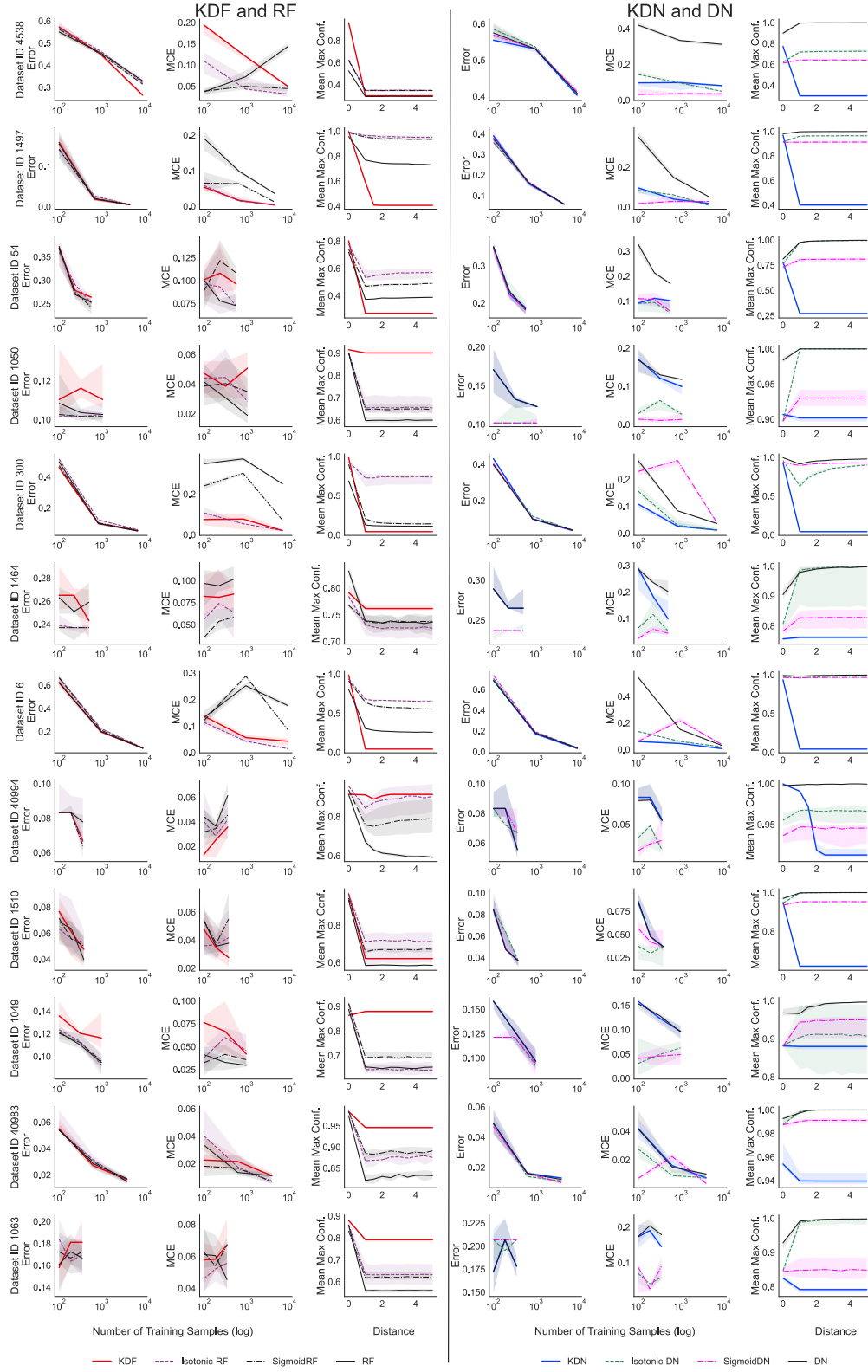


Figure 5: **Extended results on OpenML-CC18 datasets (continued).** *Left:* Performance (classification error, MCE and mean max confidence) of KDF on different Openml-CC18 datasets. *Right:* Performance (classification error, MCE and mean max confidence) of KDN on different Openml-CC18 datasets.

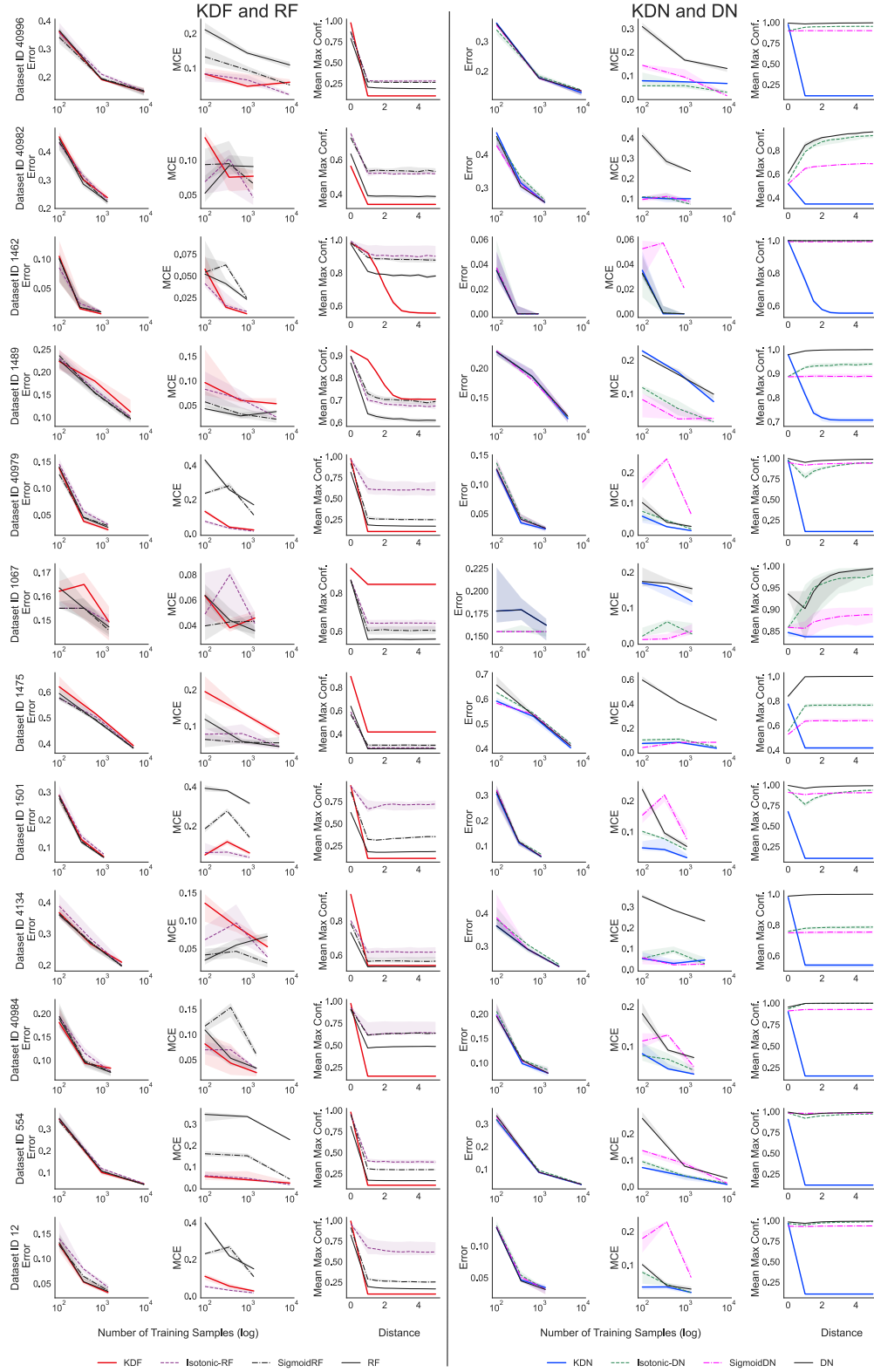


Figure 6: **Extended results on OpenML-CC18 datasets (continued).** *Left:* Performance (classification error, MCE and mean max confidence) of KDF on different Openml-CC18 datasets. *Right:* Performance (classification error, MCE and mean max confidence) of KDN on different Openml-CC18 datasets.

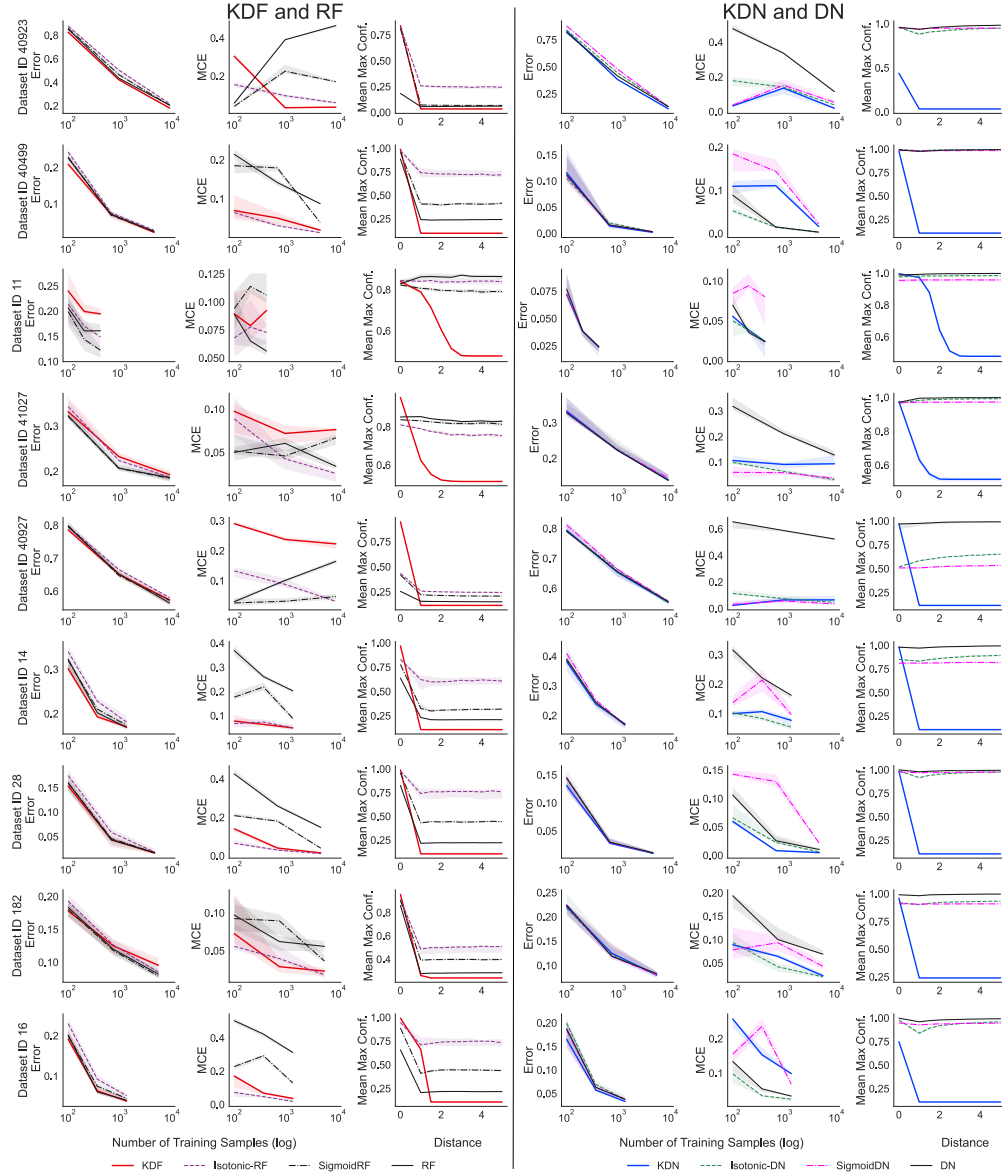


Figure 7: **Extended results on OpenML-CC18 datasets (continued).** *Left:* Performance (classification error, MCE and mean max confidence) of KDF on different Openml-CC18 datasets. *Right:* Performance (classification error, MCE and mean max confidence) of KDN on different Openml-CC18 datasets.